Supplementary Information

A Direct Probe of the Hydrogen Bond Network in Aqueous Glycerol Aerosols

Chaya Weeraratna, Chandika Amarasinghe, Wenchao Lu, Musahid Ahmed*

Chemical Science Division, Lawrence Berkeley National Laboratory, Berkeley, California 94720, USA

Table of Contents

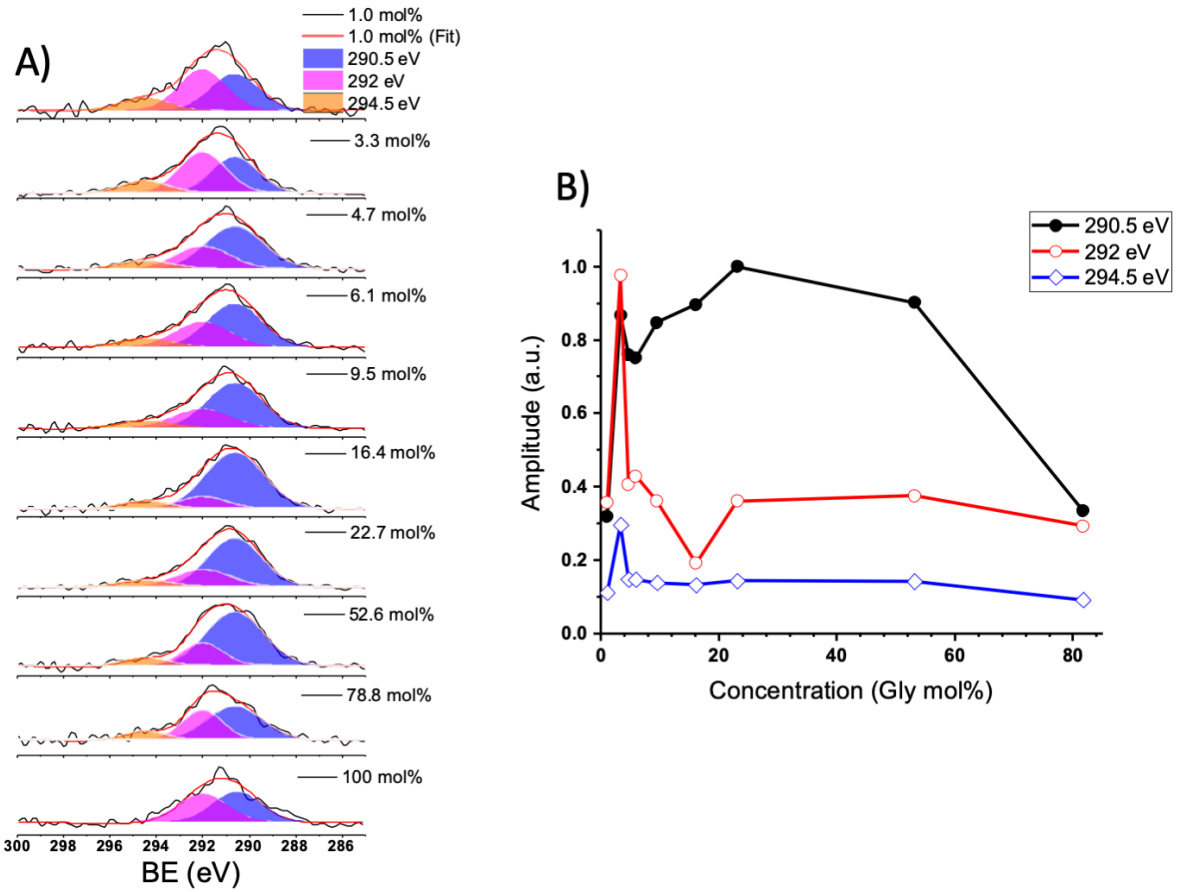

Figure S1: A) C 1s XPS spectra fitted with three gaussians. B) Intensity distribution of three gaussian peaks with concentration.

Fitting of the C 1s X-Ray photoelectron spectra to 3 gaussians: C 1s spectra was fitted with three gaussians to account for the poor fitting in the 296 – 294 eV region as discussed in the main text. The intensity distribution with concentration does not show a difference in the condensed phase (290.5 eV) and gas phase (292 eV) peak compared to the 2 peak fit.

Langmuir fitting: The C XPS intensity distribution was fitted to the Langmuir adsorption model to determine the monolayer coverage.[1]

The following equation was used;

$$N_S = \frac{N_{S,max}\,\chi_{bulk}}{\chi_{bulk} + (1 - \chi_{bulk})e^{\Delta G_{Ads}/RT}}$$

Where N_s is the contribution to the photoelectron signal from the surface of the aerosol particle as a function of glycerol concentration. $N_{s,max}$ is the maximum surface concentration, χ_{bulk} is the mol fraction of glycerol and ΔG is the Gibbs free energy.

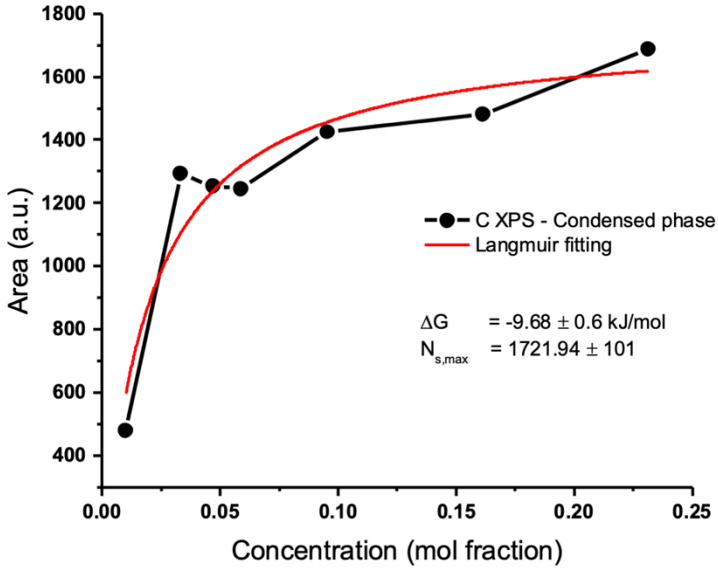

Figure S2: Langmuir fit for the C 1s intensity distribution.

NEXAFS Spectroscopy: The NEXAFS spectrum is collected to obtain the bulk measurements by replacing the camera with a photomultiplier tube (PMT). The PMT is focused to the center part of the image to collect only the high intense secondary electron signal. The photon energy is scanned between 520 – 560 eV while collecting the signal intensity and normalized by the photon flux detected from the calibrated photodiode. Similar to the XPS data collection, two data sets are acquired here as well for the signal and background.

Fig. S3 A) shows NEXAFS spectra and intensities extracted at different photon energies plotted against the glycerol-water concentration. By comparing it to the water absorption spectra from literature,[2] we can separate these spectra into three regions, pre-edge at photon energy 535 eV, main-edge at 538 eV and post-edge at 541 eV. In our case, since we have an aerosol beam, in contrast to a liquid jet or bulk liquid, our condensed phase spectra will be a convolution of liquid and ice like conditions, due to super cooling of the aerosols. Previously we have shown that NEXAFS of an water aerosol beam at the O edge,[3] could be fit approximately by a 40% liquid and 60% ice contribution. One immediate striking effect observed in the NEXAFS spectra is the absence of a pre- and post-edge peak with the main edge being dominant. This is also reflected in the plotted intensity distributions vs mol %. Since our plotted NEXAFS spectra does not immediately reflect water's X-Ray absorption spectra, even at the lowest glycerol concentration, we must assume that even the slightest addition of an alcohol perturbs the hydrogen bonding network of water typically reflected in the pre- and post-edge regions of the spectrum. NEXAFS spectroscopy generally informs on the concentration of the system under study. Hence the total intensity profile reflects how the aerosol beam concentration changes as a function of mol %. Plotted in Fig. S3 B) are the total intensity profiles, and also regions at different wavelengths to

disentangle contributions from the pre, main and post edge. Similar to the O XPS spectra, there is intensity max around 9.5 mol% concentration and then a drop followed by a plateau till mol 45 % and then dropping signal with rise in glycerol concentration. The main and post edge signal shows a peak profile similar to C XPS spectra, while the pre-edge feature shows a sharp rise followed by a much more gradual depletion in signal.

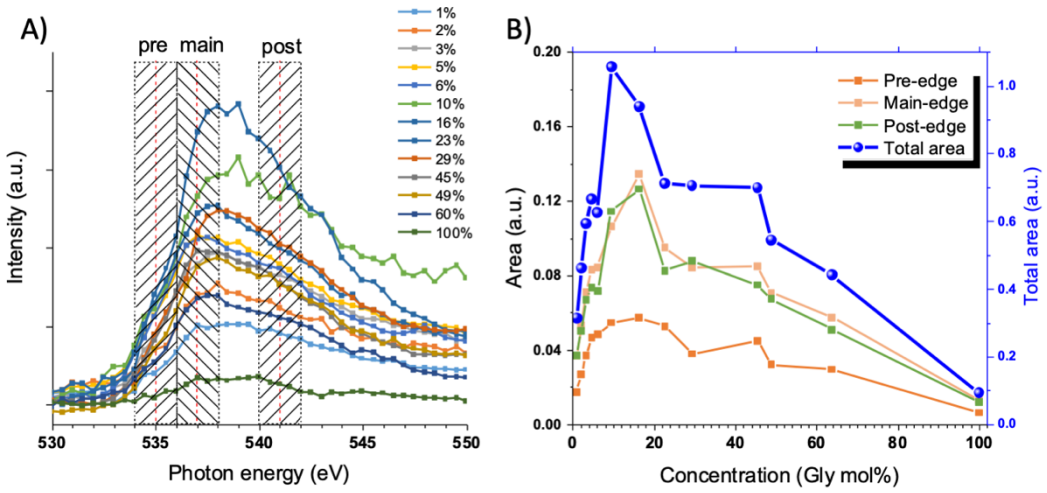

Figure S3: A) NEXAFS spectra collected for a series of concentrations including the ones used for XPS, THz and IR. Highlighted areas show the pre, main and post edge regions related to water NEXAFS spectrum. B) Areas of pre, main, post edge and total curve area plotted against concentration.

Dielectric Relaxation Measurements: The complex dielectric constant is separated to its real and imaginary part by $\varepsilon_{Debye} = \varepsilon' - i\varepsilon''$ where ε', is indicative of the extent of polarization and ε'' is the dielectric loss. These can be measured directly from the THz spectrum using the following equations.

$$\varepsilon'(\nu) = n^2 - \kappa^2 = n^2 - \frac{\alpha c}{4\pi\nu}$$

$$\varepsilon''(\nu) = \frac{n\alpha c}{2\pi\nu}$$

Where n is the refractive index, c is the speed of light and ν is the frequency. The complex dielectric constant is then easily calculated and can be simultaneously fit to the four-component Debye model given below.

$$\varepsilon_{Debye} = \varepsilon_\infty + \frac{\varepsilon_1}{2i\pi\nu\tau_1} + \frac{\varepsilon_2}{2i\pi\nu\tau_2} + \frac{\varepsilon_3}{2i\pi\nu\tau_3} + \frac{\varepsilon_4}{2i\pi\nu\tau_4}$$

Here, ε_∞ is the total dielectric strength at high frequencies, $\varepsilon_1, \varepsilon_2, \varepsilon_3$ and ε_4 are the dielectric contributions from bulk glycerol, confined water, solvated water and bulk water respectively and τ_1, τ_2, τ_3 and τ_4 are the corresponding relaxation times. The fitting was performed by fixing τ_1, τ_2, τ_3 and τ_4 to 1100 ps, 85 ps, 35 ps and 8.27 ps respectively. ε_∞ was also fixed at 7.06 and $\varepsilon_1, \varepsilon_2, \varepsilon_3$ and ε_4 was floated freely without any constraints. These parameters were obtained from the study of Charkhesht and coworkers.[4] To achieve higher accuracy, the fitting was done by using both THz data from this work and GHz data from Meaney and coworkers for the same concentrations.[5] Resulting contributions from each mechanism is then plotted as a function of glycerol concentrations in Fig. 4.

The sum of solvated and confined water contributions is compared with experimental EMV/ α_{relative} shown in Fig. S4 to demonstrate the accuracy of the fitting procedure.

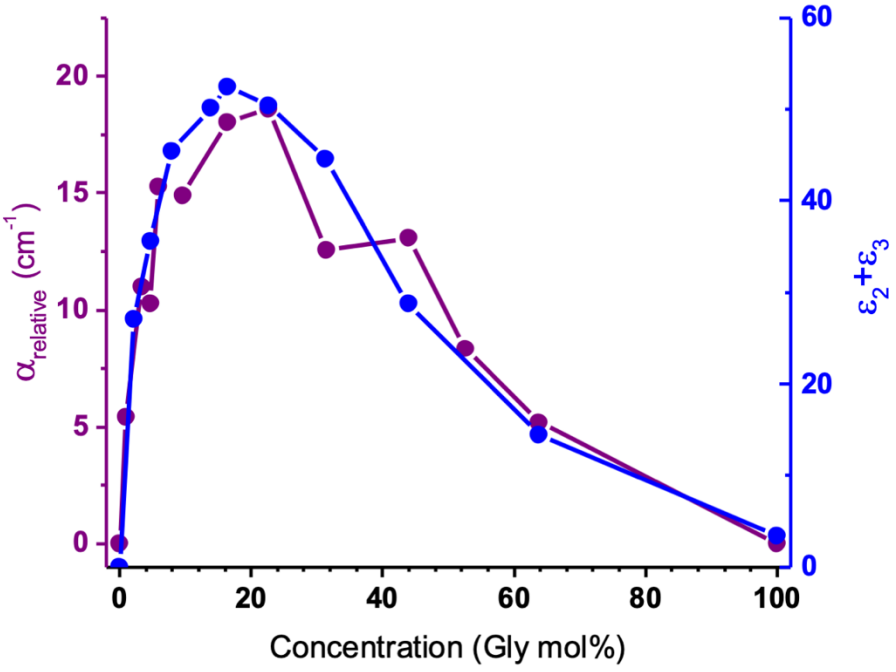

Figure S4: Comparison of EMV trends to the sum of solvated and confined water contribution.

Table S1: Intensities of condensed phase and gas phase peaks of C and O XPS spectra. In Fig. 3), C intensities are normalized by 238.5 and O intensities are normalized by 84.5.

Concentration (Gly mol%)	C XPS – 290.5 eV	C XPS – 292 eV	O XPS – 538.5 eV	O XPS – 540 eV
1.0	69.82± 3.11	93.79± 1.41	24.11± 2.88	44.77± 6.23
3.3	184.42± 7.94	255.00± 41.54	50.87± 8.35	39.27± 6.25
4.7	168.95± 1.42	132.37± 24.77	69.64± 9.74	27.88± 5.99
6.1	166.09± 5.95	127.71± 12.87	77.98± 6.49	27.17± 12.25
9.5	186.26± 7.86	118.76± 11.02	84.57± 13.25	28.54± 10.49
16.4	202.58± 19.78	54.68± 6.50	68.30± 10.47	32.67± 7.21
22.7	238.53± 35.29	111.24± 42.38	71.25± 7.88	9.08± 4.98
52.6	199.13± 18.13	106.53± 13.58	36.48± 8.89	3.75± 3.15
78.8	81.00± 5.10	68.90± 15.16	20.03± 7.31	28.70± 16.15

Table S2: $\alpha_{relative}$ values calculated at three positions and their average with concentration.

Concentration (Gly mol%)	**$\alpha_{relative}$ (cm^{-1})**			
	0.498 THz	1.011 THz	1.260 THz	Average
0	0	0	0	0
1.01	2.56	1.78	12.00	5.45± 5.69
3.3	8.49	10.01	14.44	10.98± 3.09
4.7	8.76	8.12	14.03	10.30± 3.24
6.1	12.06	15.62	18.14	15.27± 3.05
9.5	14.03	17.88	12.81	14.90± 2.65
16.4	17.35	20.11	16.70	18.06± 1.81
22.7	17.23	21.01	17.64	18.63± 2.07
31.3	13.48	13.34	10.80	12.54± 1.50
43.8	11.64	15.10	12.49	13.08± 1.80
52.6	7.96	9.52	7.58	8.35± 1.02
63.7	5.54	7.44	2.62	5.20± 2.42
100	0	0	0	0

Table S3: Dielectric strengths of each relaxation mechanism with concentration.

Concentration (Gly mol%)	Bulk water	Solvated water	Confined water	Bulk glycerol
0	74	0	0	0
2.12	51	27.08	0	0
4.65	39.71	35.64	0	0
7.79	27.48	45.4	0	0
13.8	14.46	42.04	8.1	0
16.35	12.7	37.17	15.36	0
22.67	8.93	17.15	33.29	0
31.32	7.33	0	44.58	9.09
43.87	4.16	0	28.8	32.27
63.75	2.92	0	14.48	42.45
100	2.2	0	3.45	35.14

Table S4: IR wavelength shifts of OH, CO, Asymmetric and symmetric CH_2 stretching modes with concentration.

Concentration (Gly mol%)	OH stretch (cm^{-1})	CO stretch (cm^{-1})	Asymmetric CH_2 stretch (cm^{-1})	Symmetric CH_2 stretch (cm^{-1})
0	3382.89			
1.0	3375.18	1045.34		
3.3	3373.25	1045.34		
4.6	3371.32	1043.41	2954.73	2891.08
6.1	3371.32	1043.41	2952.80	2891.08
9.5	3361.68	1043.41	2947.01	2889.15
16.1	3348.18	1041.48	2943.15	2887.22
22.7	3346.25	1041.48	2941.22	2885.29
52.6	3321.17	1039.55	2937.37	2881.44
78.8	3321.17	1039.55	2935.44	2881.44
100	3311.53	1039.55	2933.51	2879.51

References:

1. Marinho, R. R. T.; Walz, M. M.; Ekholm, V.; Ohrwall, G.; Bjorneholm, O.; de Brito, A. N. Ethanol Solvation in Water Studied on a Molecular Scale by Photoelectron Spectroscopy. *J. Phys. Chem. B* **2017,** *121* (33), 7916-7923.
2. Fransson, T.; Harada, Y.; Kosugi, N.; Besley, N. A.; Winter, B.; Rehr, J. J.; Pettersson, L. G.; Nilsson, A. X-ray and Electron Spectroscopy of Water. *Chem. Rev.* **2016,** *116* (13), 7551-69.
3. Kostko, O.; Xu, B.; Jacobs, M. I.; Ahmed, M. Soft X-ray spectroscopy of nanoparticles by velocity map imaging. *J. Chem. Phys.* **2017,** *147* (1), 013931.
4. Charkhesht, A.; Lou, D.; Sindle, B.; Wen, C.; Cheng, S.; Vinh, N. Q. Insights into Hydration Dynamics and Cooperative Interactions in Glycerol-Water Mixtures by Terahertz Dielectric Spectroscopy. *J. Phys. Chem. B* **2019,** *123* (41), 8791-8799.
5. Meaney, P. M.; Fox, C. J.; Geimer, S. D.; Paulsen, K. D. Electrical Characterization of Glycerin: Water Mixtures: Implications for Use as a Coupling Medium in Microwave Tomography. *IEEE Trans. Microw. Theory Tech.* **2017,** *65* (5), 1471-1478.